

Unveiling the nature of the highly obscured AGN in NGC 5643 with XMM-Newton

M. Guainazzi¹, P. Rodriguez-Pascual¹, A.C. Fabian², K. Iwasawa², and G. Matt³

¹*European Space Astronomy Center, RSSD of ESA, VILSPA, Apartado 50727, E-28080 Madrid, Spain*

²*Institute of Astronomy, Madingley Road, Cambridge, CB3 0HA*

³*Dipartimento di Fisica “E. Amaldi”, Università “Roma Tre”, Via della Vasca Navale 84, I-00146 Roma, Italy*

6 September 2018

ABSTRACT

We present results from an XMM-Newton observation of the nearby Seyfert 2 galaxy NGC 5643. The nucleus exhibits a very flat X-ray continuum above 2 keV, together with a prominent K_{α} fluorescent iron line. This indicates heavy obscuration. We measure an absorbing column density N_H in the range $6\text{--}10 \times 10^{23} \text{ cm}^{-2}$, either directly covering the nuclear emission, or covering its Compton-reflection. In the latter case, we might be observing a rather unusual geometry for the absorber, whereby reflection from the inner far side of a torus is in turn obscured by its near side outer atmosphere. The nuclear emission might be then either covered by a Compton-thick absorber, or undergoing a transient state of low activity. A second source (christened “X-1” in this paper) at the outskirts of NGC 5643 optical surface outshines the nucleus in X-rays. If belonging to NGC 5643, it is the third brightest ($L_X \sim 4 \times 10^{40} \text{ erg s}^{-1}$) known Ultra Luminous X-ray source. Comparison with past large aperture spectra of NGC 5643 unveils dramatic X-ray spectral changes above 1 keV. We interpret them as due to variability of the active nucleus *and* of source X-1 intrinsic X-ray powers by a factor ≥ 10 and 5, respectively.

Key words: galaxies:active – galaxies:individual (NGC 5643) – galaxies:nuclei – galaxies:Seyfert – X-rays:galaxies

1 INTRODUCTION

The X-ray spectra of Seyfert 2 galaxies exhibit significant photoelectric absorption (Warwick et al. 1989; Awaki et al. 1991; Turner et al. 1997; Risaliti et al. 1999). This evidence has been interpreted as supporting the predictions of the Seyfert unification scenarios, whereby “type 2” objects are seen at high inclination angles with respect to an azimuthally-symmetric gas and dust structure (the “torus”), which prevents us from directly observing the nucleus and the Broad Line Regions. ASCA observations, however, unveiled Seyfert 2s with peculiar X-ray spectral properties: an inverted spectrum (energy index, $\alpha < 0$); large Equivalent Width (EW) K_{α} iron fluorescent lines (EW from a few hundreds to thousands eV); very little or no evidence for photoelectric absorption (Elvis & Lawrence 1988; Koyama et al. 1989; Ueno et al. 1994). This phenomenology was interpreted as due to the column density of the absorber in this subclass of Seyfert 2s being so large, that it suppresses almost to invisibility the X-ray continuum, and enhances the contrast between the iron feature and the underlying continuum. When the absorber column density ex-

ceeds $N_H \simeq \sigma_t^{-1} = 1.5 \times 10^{24} \text{ cm}^{-2}$, the absorbing matter is optically thick to Compton scattering, and the nuclear photons are downscattered to energies where the photoelectric absorbing cross section becomes dominant. The nuclear continuum is then substantially suppressed below 10 keV, and the nucleus can be seen only along reflected and/or scattered optical paths, which do not intercept the obscuring matter. Indeed, later BeppoSAX observations, which extended the sensitive bandpass beyond 10 keV, confirmed this hypothesis by detecting nuclear emission piercing through $\gtrsim 2 \times 10^{24} \text{ cm}^{-2}$ absorbers (Matt et al. 1997b; Vignati et al. 1999; Guainazzi et al. 2000). All the above justify the nomenclature of “Compton-thick” given to this sub-class of Seyfert 2s.

The X-ray spectra of the three closest AGN (Centaurus A, NGC 4945, and the Circinus Galaxy) are absorbed by column densities larger than 10^{23} cm^{-2} , and two of them are Compton-thick. This simple fact suggests that Compton-thick Seyfert 2 galaxies may constitute a large fraction of their parent population. Indeed, BeppoSAX measurements of large samples of optically-selected Seyfert 2 galaxies suggested that they may constitute a fraction as large as 50 per

Table 1. Log of the observations discussed in this paper

Observatory-instrument/s	Date	Exposure time (ks)
ASCA-SIS/GIS	21-Feb-1996	36.7/41.5
BeppoSAX-LECS/MECS	01-Mar-1997	7.1/10.4
ROSAT-HRI	28-Aug-1997	10.0
XMM-Newton-MOS/pn	08-Feb-2002	9.4/7.1

cent of the total population (Maiolino et al. 1998, Risaliti et al. 1999), at least in the local universe. It is hard to tell whether the fraction of heavily obscured objects remains that large at cosmological distances. If so, this may have important consequences for the history of accretion, and for the total energy budget ratio between accretion and stellar light in the universe (Fabian 1999).

We have started a program to study a complete, unbiased, optically-defined sample of Compton-thick Seyfert 2 galaxies (Risaliti et al. 1999) with XMM-Newton (Jansen et al. 2001), with the main goal of characterizing their X-ray spectral properties in the hard X-ray regime. Preliminary results on the whole sample are discussed by Guainazzi et al. (2004). In this paper, we present the observation of NGC 5643. It allows us to describe in details the analysis method followed in the study of the sample. The interest of this specific observations is two-fold: a) the large collecting area of the XMM-Newton optics allows us to measure a, albeit extreme, Compton-thin absorber; b) better imaging resolution with respect to previous mission allows us to discover a serendipitous source, which apparently belongs to the optical/UV surface of the host galaxy, and outshines the nucleus. If this source is indeed associated with the NGC 5643 host galaxy, it represent one of the brightest Ultra-Luminous X-ray (ULX) source ever observed, with a total X-ray luminosity larger than 4×10^{40} erg s⁻¹.

1.1 Some properties of NGC 5643

NGC 5643 is a nearby ($z = 0.004$) SAB(rs)C galaxy, known to host a low-luminosity Seyfert 2 nucleus (Phillips et al. 1983). It exhibits an extended emission line region elongated in a direction close to the radio position angle (Morris et al. 1985), due to a "V"-shaped structure of highly excited gas. This is probably the projection of a 1.8 kpc, one-sided ionization cone (Simpson et al. 1997). Perpendicular to the radio axis, a dust lane covers the nucleus (Simpson et al. 1997). The fact that NGC 5643 belongs to the class of "extreme infrared" galaxies (Antonucci & Olszewski 1985) attracted much attention in the past to try to explain the origin of IR emission in this Active Galactic Nucleus (AGN). Although intense episodes of star formation are occurring in its nearly circular arms, evidence with respect to the nucleus is still controversial. Mid-IR diagnostics suggest that the AGN dominates the IR energy budget (Genzel et al. 1998). Comparison of optical spectra with synthesis models are, however, consistent with a "starburst/Seyfert 2 composite" spectrum (Cid Fernandes et al. 2001). The NGC 5643 nucleus is a strong radio emitter as well, most likely powered by the AGN (Kewley et al. 2000).

The log of the observations discussed in this paper is reported in Table 1. In this paper: energies are quoted in

the source reference frame; errors are at the 90 per cent confidence level for 1 interesting parameter for the best-fit model parameters, and at the 1- σ level for count rates; chemical mixture follows the Anders & Grevesse (1989) measurement; $H_0 = 70$ km Mpc⁻¹ s⁻¹ (Bennett et al. 2003). At the NGC 5643 distance (16.9 Mpc), 1'' corresponds to 82 pc.

2 XMM-NEWTON OBSERVATION

XMM-Newton (Jansen et al. 2001) observed the sky region encompassing NGC 5643 on February 8, 2003. The X-ray imaging EPIC cameras (pn, Strüder et al. 2001; MOS, Turner et al. 2001) were operated in Full Frame Mode, with the MEDIUM optical photons blocking filter. The Optical Monitor (OM; Mason et al. 2001) was operated in standard Image Mode with the UVW1 filter, sensitive in the 2500-4000Å bandpass. Data reduction was performed with version 5.4.1 of the SAS software package (Jansen et al. 2001). We employed the most updated calibration files available at the time the reduction was performed (June 2003). None of the X-ray sources discussed in this paper was detected by the high-resolution spectroscopy camera, RGS (der Herder et al. 2001). Standard data screening criteria were applied in the extraction of scientific products. The particle background stayed at a quiescent level (Lumb et al. 2002) during the whole observation, making unnecessary any background-rejection filtering. Pattern 0 to 4 (12) were employed in the extraction of pn (MOS) scientific products. Spectra and light curves were extracted from circular regions of 25'' radius around the source centroids. Response matrices, appropriate for each of the spectra discussed in this paper, were generated with the SAS tasks `arfgen` and `rmfgen`. Background spectra were extracted from source-free regions of the same CCD as where the source is located. Spectra were rebinned to ensure that: a) the instrumental energy resolution is over-sampled by a factor not larger than 3; b) at least 25 (50) counts are present in each MOS (pn) spectral channel, to ensure the applicability of the χ^2 statistics in the evaluation of the fit quality. Images, spectra and response matrices of the two MOS cameras were combined together, to increase signal-to-noise. Spectral fits were performed simultaneously on both EPIC cameras, using the 0.35–12 and 0.5–10 keV energy bands for the pn and the MOS, respectively. As no significant variability was detected during the XMM-Newton observation, in this paper we will discuss the time-averaged spectra only.

In Fig. 1 the 0.5–10 keV sky coordinates MOS image of the innermost 3' around the NGC 5643 nucleus is shown. Four sources are detected by the EPIC cameras in this field at a signal-to-noise ratio larger than 3. The source detected at ($\alpha_{2000} = 14^h 32^m 40.9^s$, $\delta_{2000} = -44^\circ 10' 26''$) coincides with NGC 5643 optical nucleus within the typical XMM-Newton attitude reconstruction accuracy. Its total counts are 1380 ± 40 and 640 ± 30 in the pn and MOS camera, respectively. The source located $\simeq 0.8'$ NE the nucleus is 50 per cent brighter than the nucleus. We will refer to it as "NGC 5643 X-1" hereafter. Its total counts are 2030 ± 60 and 1320 ± 40 in the pn and MOS cameras, respectively.

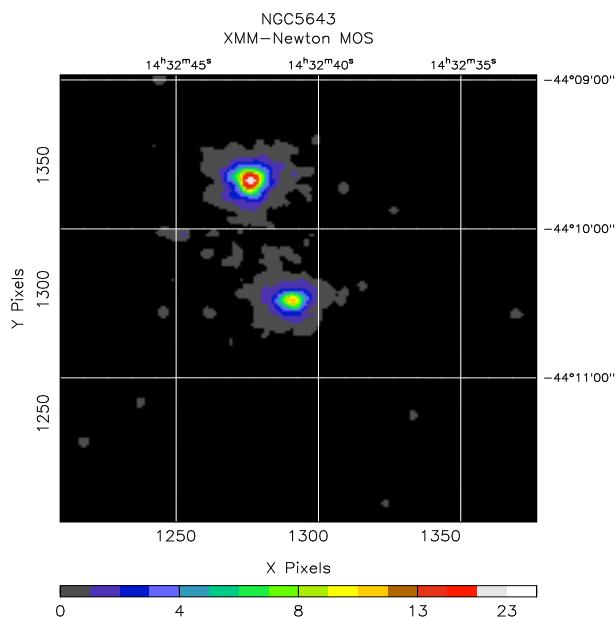


Figure 1. 0.5–10 keV single- and double-events MOS image, restricted to the $3'$ around the NGC 5643 optical nucleus. The image is smoothed with a Gaussian function ($\sigma = 1.5''$). The scale is in units of unsmoothed pixel counts.

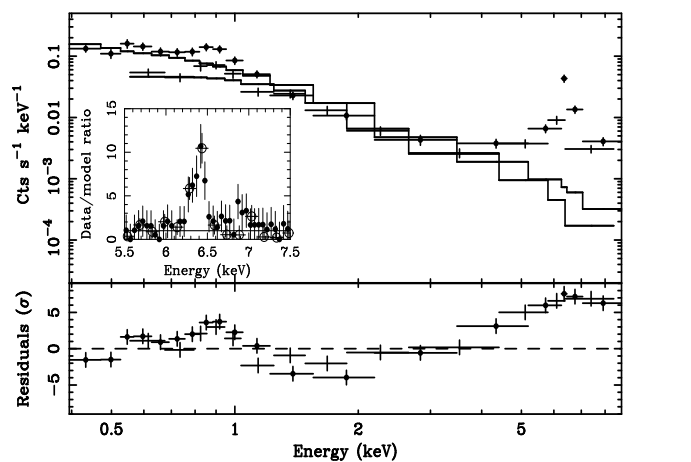


Figure 2. NGC 5643 nucleus EPIC spectra (*upper panel*; dots: pn; crosses: MOS) and residuals in units of standard deviations (*lower panel*) against a power-law model. In the *inset*: data/model ratio in the 5.5–7.5 keV energy band against a power-law model above 2 keV (pn: *filled circles*; MOS *empty squares*). In the latter panel, data are rebinned according to a constant factor $\delta E = 50$ eV for plotting purposes only

2.1 Spectral analysis of the nucleus

In Fig. 2 we show the result of a power-law fit^{*} on the NGC 5643 nucleus spectrum. The fit is clearly unacceptable ($\chi^2/\nu = 417.0/29$). As often observed in highly absorbed

^{*} All the models employed in this paper include photoelectric absorption by a column density due to the contribution of neutral matter in our Galaxy along the line-of-sight to NGC 5643: $N_{H, Gal} = 8.3 \times 10^{20} \text{ cm}^{-2}$ (Dickey & Lockman 1990)

Seyfert 2 galaxies (Matt et al. 2000) the residuals exhibit a “turning point” around 2 keV, suggesting that the continuum needs to be modeled with (at least) two components. Additionally, a broad excess emission feature is localized around $E \simeq 0.85$ keV (observer’s frame), together with a narrow emission feature around 6 keV. In order to achieve a full physical characterization of the overall spectrum, we have first separately analyzed the regimes above and below the spectral “turning point”.

2.1.1 The soft X-ray spectrum ($E < 2$ keV)

The soft energy spectrum is remarkably complex. A fit with a single featureless continuum in the energy band redwards of 1 keV is clearly inadequate (*e.g.*: $\chi^2_\nu \simeq 3.5$ if a power-law is employed), and leaves large positive residuals in the energy range between 0.8 and 1 keV. In this region a “forest” of iron-L transitions exists. At least two thermal components[†] are required in order to adequately account for this feature, with temperatures $kT_s \simeq 0.17$ keV and $kT_h \simeq 0.69$ keV ($\chi^2/\nu = 9.7/8$). Alternative “two continuum components” descriptions of the soft X-ray spectrum are possible, and yield statistically equivalent fit, such as the combination of thermal emission and power-law ($kT \simeq 1.1$ keV; $\Gamma \simeq 2.2$), or of thermal and multi-temperature accretion disk blackbody emission (model `diskbb` in XSPEC; $kT^{thermal} \simeq 90$ eV; $kT^{disk} \simeq 1.0$ keV).

Is it alternatively possible that the soft X-ray spectrum is dominated by scattering? The soft X-ray spectrum can be in principle reasonably fit with a combination of a, say, power-law continuum plus three emission lines ($\chi^2_\nu \simeq 1.23$). However the spectral index in this scenario ($\Gamma \simeq 4.0$) is too steep to represent the mirror of the AGN intrinsic continuum, even if self absorption effect in the scattering plasma are neglected. However, high-resolution grating measurements of bright absorbed Seyfert galaxies are showing that the soft X-ray emission is often dominated by heavily blended emission lines (Kinkhabwala et al. 2002; Brinkmann et al. 2002; Sako et al 2000). The blend can mimic continuum emission - alongside a few emission “peaks” corresponding to the brightest well defined lines - in low-resolution spectra (Guainazzi et al. 1999; Cappi et al. 1999). Testing this hypothesis would require high-resolution good quality spectroscopic data, which are not available for the NGC 5643 nucleus. Nonetheless, we fit the EPIC spectra with a combination of emission lines only, aiming at inferring the main qualitative properties of the line emitting plasma in this scenario. In order to avoid line blurring effects induced by spectral rebinning, we fit the unbinned spectrum, using the C-statistics (Cash 1976). Only the pn spectrum was used, due to larger effective area. No background subtraction was performed, as its contribution is ≤ 10 per cent in the soft X-ray band. Seven lines are required to fit the spectrum (see Fig. 3, and Table 2). Typical statistical uncertainties on their centroid energy are $\simeq 10$ eV (except for the highest energy

[†] hereafter thermal emission from an optically thin, collisionally excited plasma is modeled via the code `mekal` in XSPEC (Mewe et al. 1985). Unless otherwise specified, the plasma abundance has been kept fixed to $Z = 0.5Z_\odot$

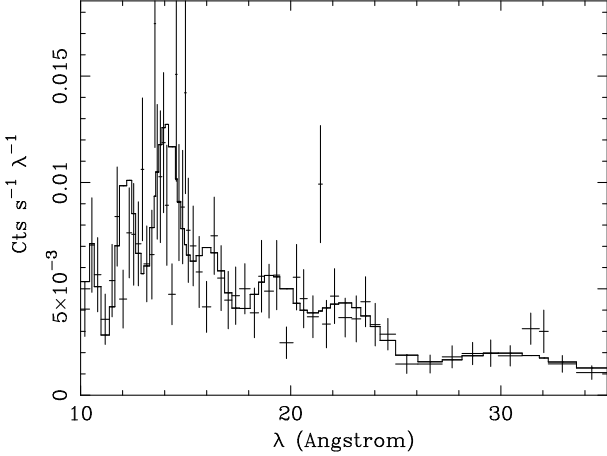


Figure 3. 10–35Å pn spectrum (*crosses*) superposed to the emission-line only model best-fit (*solid line* - details in text)

Table 2. Centroid energies for the measured emission lines, if the soft X-ray pn spectrum of the NGC 5643 nucleus is fit with a model constituted by emission lines only. The *right column* shows the possible identifications. They take into account the statistical uncertainties on the centroid energies only. In brackets, additional identifications are listed when systematics uncertainties are taken into account as well. RRC = Radiative Recombination Continuum

Energy (keV)	Identifications
0.428	CVI β (NVI)
0.566	OVI
0.668	OVI γ
0.787	FeXVII
0.899	NeIX, FeXIX
1.028	NeIX β , FeXXII
1.176	NeIX RRC, FeXXIV

line in Table 2, for which they are $\simeq 20$ eV). Systematic uncertainties on the gain are of the same order.

Better data quality is necessary to achieve a fully unambiguous deconvolution of the soft X-ray spectrum. For sake of simplicity, we will assume in the following a modeling of the soft X-ray spectrum in terms of a two-component optically-thin thermal plasma.

2.1.2 The hard X-ray spectrum ($E > 2$ keV)

The nuclear spectrum above 2 keV is no less complex. A formally adequate fit is achieved through an unabsorbed power-law and an emission line (parameterized through a simple Gaussian profile). The latter is required at the 99.87 per cent confidence level according to the F-test. However, the best-fit parameters suggest that this is no more than a purely mathematical description. The power-law spectral index is inverted (photon index, $\Gamma \simeq -0.8$), what is totally unusual for AGN (Nandra et al. 1997; et al. 1997; Reeves & Turner 2000; Perola et al. 2002). The emission line centroid energy ($E_c \simeq 6.42$ keV) is consistent with K_{α} fluorescent emission from neutral or mildly ionized iron. The formal

line Equivalent Width is huge: $EW \simeq 2.8$ keV (cf. the inset in Fig. 2).

Flat hard X-ray spectra with huge EW K_{α} fluorescent iron lines in Seyfert 2 galaxies can be produced if the bulk of hard X-ray emission is due to Compton-reflection of an otherwise invisible “standard” AGN nuclear continuum, either because the AGN switched to an “off” state during the XMM-Newton observation, or because its emission is totally suppressed by a Compton-thick absorber (Matt et al. 2003). We have therefore fit the EPIC nuclear spectra in their full energy bandpasses with a combination of two thermal components, a Gaussian emission line, and a “bare” Compton-reflection component (model *pe xrav* in XSPEC; Magdziarz & Zdziarski 1995). The fit is unacceptable ($\chi^2/\nu = 49.9/22$), mainly due to large excess residuals between 2 and 5 keV. This excess could be in principle due to optically thin electron scattering of the otherwise invisible nuclear continuum. Indeed, adding a power-law component yields a statistically acceptable fit ($\chi^2/\nu = 18.6/21$). However, the spectral index of this power-law is too flat ($\Gamma = -0.1 \pm 0.6$), for its interpretation as the “warm mirror” of the nuclear continuum to be plausible. The combination of a Compton-thick absorber with nuclear electron scattering can be therefore ruled out.

A possible alternative is that the Compton-reflection component is in turn absorbed by matter with a covering fraction lower than 1. In this case, the 2–5 keV spectrum is accounted for by $\simeq 5\%$ of the Compton-reflection continuum (see Model#1 in Table 3) which “leaks” through its absorber. This leakage has the appropriate flatness. An absorber with a $\simeq 95$ per cent covering fraction and $N_H = (1.0 \pm 0.3) \times 10^{24} \text{ cm}^{-2}$ is required in this scenario. If the hard X-ray continuum is dominated by Compton-reflection, K_{α} emission lines from O to Cr are expected to imprint their signatures along with the Fe line. They are not detected in the EPIC spectra of NGC 5643. However, their EW upper limits (200–300) eV are inconclusive (Matt et al. 1997b).

The depth of the K photoelectric absorption edge is in principle a powerful diagnostic for the metallicity of the absorbing and/or reflecting matter. A further 97 per cent confidence level improvement in the quality of the fit ($\Delta\chi^2/\Delta\nu = 5.0/1$) is obtained in Model#1 of Table 3 if the iron metallicity is left free. If this change is attributed to one of the two components only (what is unlikely, if absorber and reflector represent one and the same system; see Sect. 4.1): $Z_{Fe} \leq 0.7Z_{\odot}$.

Alternatively, Compton-thin obscuration - still allowing a fraction of the direct nuclear emission to pierce through the X-ray absorber in the EPIC energy bandpass - can as well significantly harden a typical AGN spectrum. We have therefore substituted the partially covered Compton-reflection component with a power-law modified by photoelectric absorption. Again the fit is statistically acceptable ($\chi^2_{\nu} \simeq 0.95$). The best-fit models results are reported in Table 3. In this scenario the 2–5 keV excess can be accounted for by optically-thin scattering of the nuclear continuum, with a reasonable spectral shape ($\Gamma = 1.4 \pm 0.7$). The extrapolation of the scattered nuclear continuum into the 0.4–1.2 keV band is $\simeq 15$ per cent in Model #3. No significant evidence is found for a deviation of the absorber metallicity from standard solar abundances in this scenario: $Z_{Fe} = 0.8 \pm 0.6 Z_{\odot}$. In Model#2 of Table 3 the electron scat-

Table 3. Best-fit parameters and results for the EPIC NGC 5643 nuclear spectrum. Model #1 is constituted by the combination of two thermal components (with temperatures kT_s , and kT_h), a Compton-reflection continuum, partly absorbed by matter with a covering fraction f_c and column density N_H , and a Gaussian emission line profile with centroid energy E_c , intensity I_{line} , and Equivalent Width EW . Model #2 is constituted by the combination of three thermal components (the hottest with temperature kT_{uh}), an absorbed power-law, and the Gaussian emission line profile. In Model #3 the “ultra-hard” thermal component is substituted by a locally unabsorbed power-law. f_s is defined as the scattering fraction between the transmitted and the scattered nuclear component in Model #3

Parameter	Model #1	Model #2	Model #3
Γ	$2.3^{+0.9}_{-1.0}$	$1.6^{+1.0}_{-1.9}$	$1.4^{+0.7}_{-0.2}$
N_H (10^{23} cm $^{-2}$)	10 ± 3	6 ± 4	7 ± 2
f_c or f_s (per cent)	$94.7^{+3.4}_{-5.6}$...	$3.3^{+7.3}_{-2.8}$
E_c (keV)	$6.39^{+0.04}_{-0.05}$	$6.43^{+0.02}_{-0.05}$	$6.43^{+0.02}_{-0.05}$
I_{line}^a	8 ± 4	1.4 ± 0.4	$1.5^{+0.4}_{-0.3}$
EW (eV)	760	490	500
kT_s (keV)	$0.17^{+0.07}_{-0.08}$	$0.15^{+0.03}_{-0.07}$	$0.15^{+0.03}_{-0.07}$
kT_h (keV)	$0.73^{+0.10}_{-0.08}$	0.67 ± 0.05	$0.67^{+0.05}_{-0.04}$
kT_{uh} (keV)	...	> 5	...
0.5–2 keV flux b	2.16 ± 0.15
2–10 keV flux b	$8.4^{+1.3}_{-1.2}$
χ^2/ν	21.2/19	20.0/21	20.8/22

a in units of 10^{-5} cm $^{-2}$ s $^{-1}$

b corrected for Galactic absorption, in units of 10^{-13} erg cm $^{-2}$ s $^{-1}$

tering is substituted by a “ultra-hot” ($kT \simeq 5$ keV) thermal component.

In order to investigate the details of the iron line structure, we have performed a Cash statistic fit of the unbinned pn spectrum in the 4–8 keV energy range, again to prevent the line profile from being blurred by the χ^2 applicability requirement. The contribution of the background has been estimated by fitting the background spectrum in the same energy band with a simple power-law. The best-fit parameters for the background are: $\Gamma = 3.08$ and 1 keV normalization, $N = 5.8 \times 10^{-5}$ cm $^{-2}$ s $^{-1}$. The source spectrum continuum was then fitted with a double power-law, one of the two components having its parameters fixed to the background best-fit model. Two lines are detected in the spectrum, at a confidence level larger than 99 per cent for 1 interesting parameter (see Fig. 4; Lampton et al. 1976). They have centroid energies $E_1 = 6.40 \pm 0.02$ keV and $E_2 = 6.93 \pm 0.05$ keV, and intensities $(1.4 \pm 0.4) \times 10^{-5}$ cm $^{-2}$ s $^{-1}$, and $(4 \pm 3) \times 10^{-6}$ cm $^{-2}$ s $^{-1}$, respectively. The fainter line is consistent with K_α fluorescence of H-like iron.

The observed fluxes - calculated according to Model #3 best-fit parameters in Table 3 - are 1.7×10^{-13} and 8.3×10^{-13} erg cm $^{-2}$ s $^{-1}$ in the 0.5–2 keV and 2–10 keV energy ranges, respectively. The corresponding luminosity in the 0.5–2 keV energy range, once corrected for the Galactic absorption, is $\simeq 9 \times 10^{39}$ erg s $^{-1}$. The intrinsic AGN luminosity, further corrected for its local absorption, is $(2.5^{+2.2}_{-2.0}) \times 10^{41}$ erg s $^{-1}$ in the 0.5–10 keV energy range.

2.2 Spectral analysis of NGC 5643 X-1

In Fig. 5 we show the EPIC spectra of NGC 5643 X-1 and its

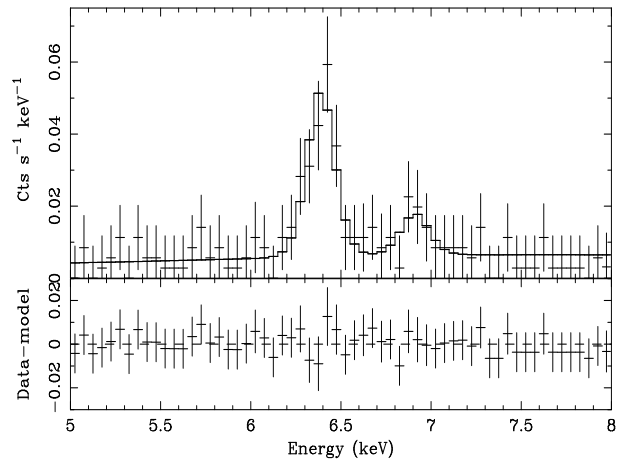


Figure 4. Upper panel: pn spectrum (crosses) and best-fit model (solid line) in the 4–8 keV energy band, showing two emission lines with centroid energies $\simeq 6.40$ keV and $\simeq 6.93$ keV. Lower panel: residuals against the best-fit model. A constant $\delta E = 50$ eV rebinning has been applied for plotting purposes only

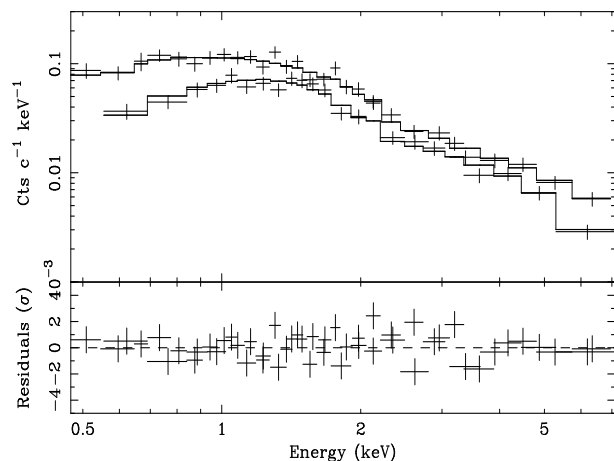


Figure 5. Spectra (upper panel) and residuals in units of standard deviation (lower panel), against a photoelectrically absorbed power-law for NGC 5643 X-1

best-fit with a photoelectrically absorbed power-law model. This fit is acceptable ($\chi^2/\nu = 46.4/48$). An equally good fit can be obtained with a thermal bremsstrahlung continuum. A fit with a multitemperature blackbody (`diskbb` in XSPEC) is instead poor. A summary of the best-fit parameters and results is shown in Table 4. No iron K_α fluorescent emission line (or any other narrow band features) is detected in the spectrum. The upper limit on the EW of a “narrow” (*i.e.* $\sigma \equiv 0$), neutral ($E_c \equiv 6.4$ keV in the observer’s frame) line is 270 eV.

The observed flux in the 0.5–10 keV energy band is $(1.11 \pm 0.06) \times 10^{-12}$ erg cm $^{-2}$ s $^{-1}$. It corresponds to an intrinsic luminosity of $(4.4 \pm 0.2) \times 10^{40}$ erg s $^{-1}$ if NGC 5643 X-1 is located at the galaxy redshift.

Table 4. Best-fit parameters and results for the NGC 5643 X-1 EPIC spectra. Models legenda: **po** = power-law; **diskbb** = multi-temperature disk blackbody; **brems** = thermal bremsstrahlung,

Parameter	po	diskbb	brems
$N_H(10^{21} \text{ cm}^{-2})$	1.7 ± 0.4	<0.05	$1.1 \pm_{0.3}^{0.2}$
Γ	$1.69 \pm_{0.10}^{0.09}$
kT (keV)	...	$1.42 \pm_{0.09}^{0.08}$	$8.5 \pm_{1.7}^{2.2}$
0.5–2 keV flux ^a	4.4 ± 0.5
2–10 keV flux ^a	7.5 ± 0.6
χ^2/ν	46.3/48	87.8/48	45.9/48

^aabsorption-corrected, in units of $10^{-13} \text{ erg cm}^{-2} \text{ s}^{-1}$

Table 5. Sources detected in the ROSAT/HRI observation of the NGC 5643 field, within 3' the optical nucleus at a signal-to-noise ratio larger than 3

α_{2000}	δ_{2000}	Count rate (10^{-3} s^{-1})	Flux ^a
$14^{\text{h}}32^{\text{m}}40.7^{\text{s}}$	$-44^{\circ}10'24''$	7.1 ± 1.0	2.3 ± 0.3
$14^{\text{h}}32^{\text{m}}41.9^{\text{s}}$	$-44^{\circ}09'36''$	3.2 ± 0.7	1.5 ± 0.3

^a0.5–2 keV flux in units of $10^{-13} \text{ erg cm}^{-2} \text{ s}^{-1}$, absorption-corrected and extrapolated from the measured count rate via the HEASARC on-line tool PIMMS, using the best-fit models of the XMM-Newton observation

3 THE X-RAY HISTORY OF NGC 5643

In this Section we compare the results of the XMM-Newton observation of the NGC 5643 field with earlier ASCA, BeppoSAX, and ROSAT/HRI observations. Data were retrieved from the NASA/HEASARC and ASI/ASDC archival facilities, and reduced according to standard procedures. In the HRI image both NGC 5643 XMM-Newton sources are individually detected, thanks to its good spatial resolution (see Table 5) On the other hand, the broad Point Spread Function of the ASCA and BeppoSAX optics mixes irretrievably the contribution of the two sources in their typical aperture. In both latter cases, we analyzed a single spectrum extracted from a circular region of 3' radius (except for the BeppoSAX LECS detector, for which an aperture of 2' was used due to the lack of appropriate calibrations). Spectra were rebinned according to the same criteria employed for the XMM-Newton/MOS spectra (cf. Sect. 2.1). Background spectra were extracted from nearby regions in the same field-of-view where the source is located. The soft flux exhibits a dynamical range of about a factor 2 between the ASCA (faintest) and the XMM-Newton (brightest) state. The variation amplitude in the hard X-rays is somewhat smaller ($\simeq 30$ per cent).

Is it possible to unambiguously ascribe the observed historical flux variability either to the NGC 5643 nucleus or to source X-1? The fainter states caught by BeppoSAX and - above all - ASCA may represent a “diluted” version of a more dramatic variability affecting only one of the members of the pair. Indeed, NGC 5643 X-1 underwent a factor of 3 variation in flux between the 1997 ROSAT/HRI and the 2002 XMM-Newton observations. However, a quantitative assessment of this issue across the whole X-ray history of NGC 5643 is not straightforward.

The ASCA and BeppoSAX spectra exhibit mutually

Table 6. Best-fit parameters and results for the ASCA and BeppoSAX spectra of the 3' radius region encompassing NGC 5643. The best-fit continua are: **mekal** plus power-law for ASCA, and power-law for BeppoSAX, respectively. Both models include a narrow Gaussian profile, and absorption by a column density $N_{H,Gal} = 8.3 \times 10^{20} \text{ cm}^{-2}$.

Parameter	ASCA	BeppoSAX
Γ	1.04 ± 0.14	$1.9 \pm_{0.3}^{0.4}$
kT (keV)	$0.68 \pm_{0.09}^{0.10}$...
E_c (keV)	6.45 ± 0.11	$6.43 \pm_{0.16}^{0.10}$
EW (keV)	1.7 ± 0.4	$1.9 \pm_{1.0}^{1.4}$
0.5–2 keV flux ^a	$3.3 \pm_{0.4}^{0.5}$	$5.4 \pm_{1.4}^{1.6}$
2–10 keV flux ^a	9.8 ± 1.5	10 ± 2
χ^2/ν	131.0/184	9.1/13

^aabsorption-corrected, in units of $10^{-13} \text{ erg cm}^{-2} \text{ s}^{-1}$

different spectral shapes, notwithstanding the universal presence of the large EW K_{α} fluorescent iron line (see Fig. 6). A simple power-law continuum is an adequate representation of the BeppoSAX spectrum, with a steep index ($\Gamma = 1.9 \pm_{0.3}^{0.4}$). This is markedly discrepant with the photon index measured by XMM-Newton, when a simple power-law is applied above 2 keV ($\Gamma \simeq -0.8$; cf. Sect. 2.1.2). The ASCA spectra requires at least two continuum components. Adopting for simplicity the combination of a thermal and a power-law component, the temperature of the former is consistent with kT_h as measured by XMM-Newton, whereas the latter’s spectral index is intermediate between BeppoSAX and XMM-Newton ones. A summary of the ASCA and BeppoSAX best-fits - which represent for each case only one of the possible statistically equivalent solutions - is reported in Table 6.

In order to quantitatively estimate the differences with respect to the XMM-Newton measurements, we have built a “composite” XMM-Newton spectrum, combining the best fit models for the NGC 5643 nucleus and source X-1. This “composite” spectrum is shown in Fig. 7, whereas the ratios between the ASCA and BeppoSAX spectra and the “composite” spectrum are shown in Fig. 6. Both these ratios are consistent with 1 below 1 keV. Above 1 keV their behaviors differ: the ratio against the BeppoSAX spectrum decrease monotonically up to 10 keV; the ASCA ratio remains basically constant around a value of about 0.6, with a local excess around the iron K_{α} iron line.

In principle, applying this “composite” model to the ASCA and BeppoSAX spectra should provide the ultimate answer to the question on which source in the NGC 5643 field is responsible for the flux and spectral variations observed across the X-ray history of NGC 5643. Unfortunately, the composite model has too many parameters, and would therefore largely overfit the ASCA and BeppoSAX spectra. We have therefore limited the scope of the exercise, keeping all the parameters of the composite model frozen to the XMM-Newton values, except the continua and iron line normalizations. This represents of course a very crude (and admittedly arbitrary) assumption. The results of this exercise are summarized in Table 7. Its main conclusions can be outlined as follows:

- the ASCA soft X-ray faint state might be mainly due

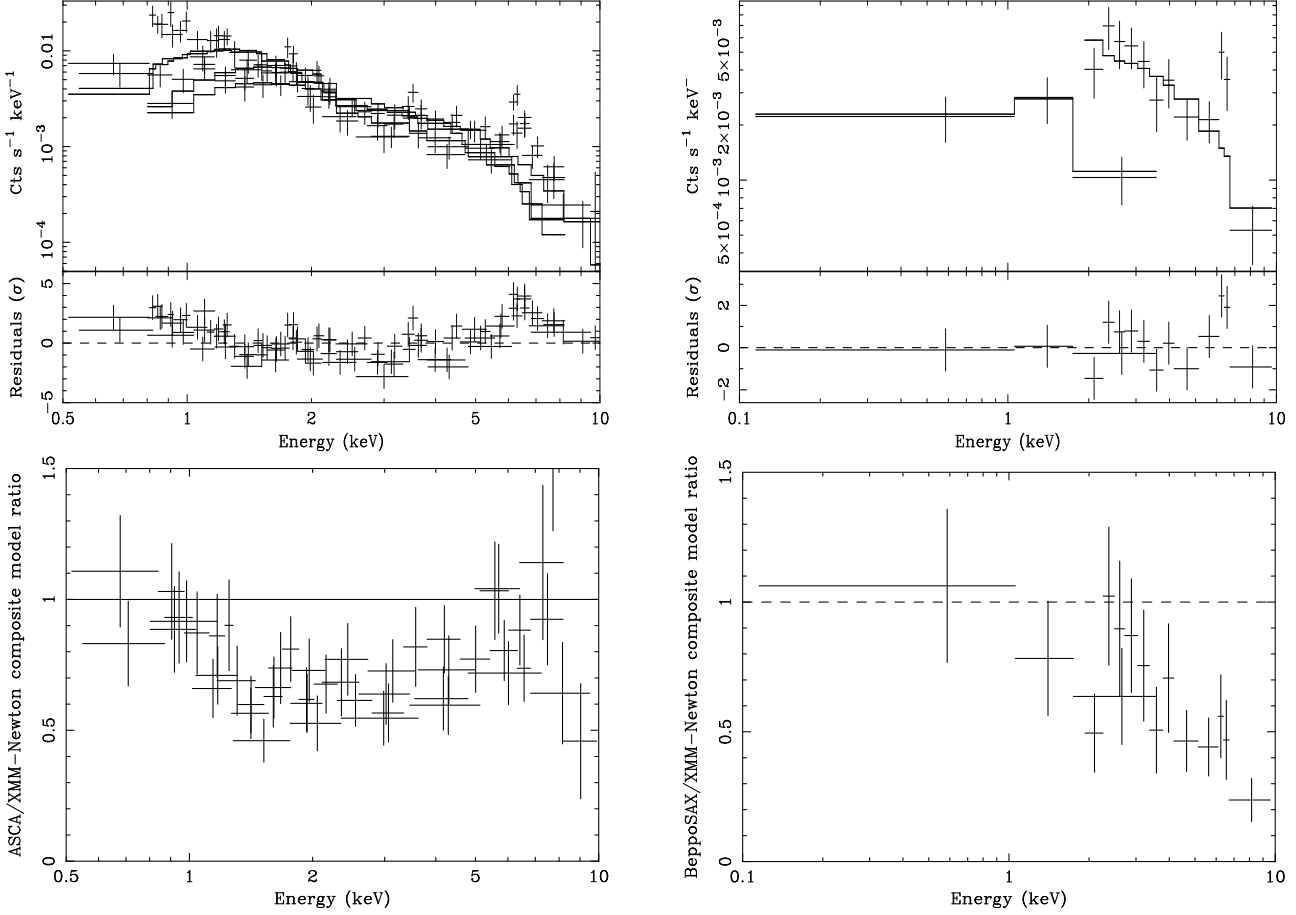


Figure 6. Top: spectra (*upper panels*) and residuals in units of standard deviation (*lower panels*), when the ASCA (*left*) and BeppoSAX (*right*) spectra are fit with a power-law model. Bottom: ratio between the ASCA and BeppoSAX spectra and the XMM-Newton “composite” model (details in text).

Table 7. Continua and iron line normalizations when the “composite” model is applied to the ASCA and BeppoSAX spectra. The XMM-Newton best-fit values are shown as well for comparison. Legend: $N_{pl,a}$: normalization of the locally absorbed power-law; $N_{pl,u}$: normalization of the locally unabsorbed power-law; $N_{th,s}$: normalization of the softer thermal component; $N_{th,h}$: normalization of the harder thermal component. The superscripts n and X^{-1} refers to the NGC 5643 nucleus and sources X-1, respectively. Errors are at 1- σ level for 1 interesting parameter. Values are expressed as $\times 10^{-5}$ of the corresponding units. Power-law normalizations are at 1 keV

Normalization	ASCA	BeppoSAX	XMM-Newton
$N_{pl,a}^n$	7.2 ± 1.9	< 0.6	$8.1 \pm_{1.0}^{0.8}$
$N_{pl,u}^n$	$0.81 \pm_{0.40}^{0.04}$	< 0.5	0.27 ± 0.02
$N_{pl,a}^{X^{-1}}$	< 0.4	1.4 ± 0.6	1.97 ± 0.05
$N_{th,s}^n$	4 ± 3	< 18	$2.5 \pm_{0.3}^{0.2}$
$N_{th,h}^n$	0.7 ± 0.2	$1.6 \pm_{1.6}^{0.7}$	0.83 ± 0.05
I_{line}^n	1.8 ± 0.3	$2.0 \pm_{1.2}^{0.8}$	$1.6 \pm_{0.2}^{0.3}$

to source NGC 5643 X-1 becoming at least five times fainter than during the XMM-Newton (or BeppoSAX) observation

- the hard X-ray steep BeppoSAX spectrum might be mainly due to a decrease of the flux associated with the

nuclear emission, leaving source X-1 as the dominant contributor to the hard X-ray flux

It is worth noticing that the intensity of the iron line is consistent with being constant across all the observations.

Given the crudeness of the above assumption, these conclusions must be regarded as no more than hints to the true physical picture. The ultimate answer on the nature of the X-ray variability in this system must await future re-observations with either *Chandra* or XMM-Newton.

4 DISCUSSION

4.1 The nature of the obscured AGN in NGC 5643

A qualitative difference exists between objects obscured by matter with a column density smaller (Compton-thin) or larger (Compton-thick) than $N_H \simeq \sigma_t^{-1} \simeq 1.5 \times 10^{24} \text{ cm}^{-2}$ at energies lower than 10 keV, where most of the X-ray detectors flown so far were sensitive. Compton-thick AGN can be observed only along optical paths, which do not intercept the absorbing matter. This may make highly uncertain the determination of their intrinsic luminosity, which is dependent on the largely unknown distribution and covering frac-

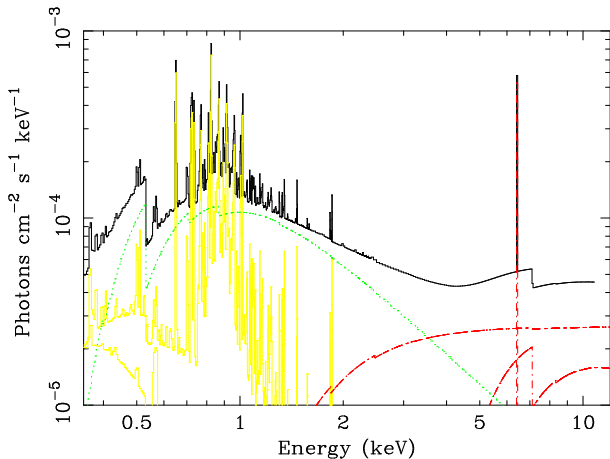


Figure 7. XMM-Newton “composite” spectrum, combining NGC 5643 nucleus (Model #3 in Table 3), and X-1 source best-fits. *Pale solid lines:* thermal components; *dashed lines:* AGN continuum and K_{α} iron fluorescent line; *dotted line:* X-1 best-fit power-law; *thick, upper solid line:* total composite spectrum

tion of the reflecting and/or scattering matter. Even more importantly, a Compton-thick absorber substantially suppresses the incident radiation even at energies larger than the photoelectric cut-off. At 30 keV (100 keV), the fraction of transmitted radiation with respect to an absorber with $N_H = 10^{23.75} \text{ cm}^{-2}$ is about 85, 30, 4 per cent (50, 20, 2 per cent) for $N_H = 10^{24.25} \text{ cm}^{-2}$, $10^{24.75} \text{ cm}^{-2}$, $10^{25.25} \text{ cm}^{-2}$, respectively (Wilman & Fabian 1999). Knowing how many Compton-thick AGN exist may have an impact on the history of accretion in the universe (Fabian 1999)

Previous BeppoSAX observations suggested that Compton-thick objects represent a large fraction of the Seyfert 2 population (Maiolino et al. 1998), maybe as large as 30–50 per cent (Risaliti et al. 1999). To identify Compton-thick AGN, the measurement of two critical observables was required: the shape of the power-law continuum above 2 keV, and the EW of the K_{α} iron line. Observed flat spectra ($\Gamma \leq 1.0$), and large EW (\geq a few hundreds eV) have been considered signatures of a reflection-dominated (*i.e.*, Compton-thick) AGN. In principle, a detection by the BeppoSAX PDS above 15 keV was crucial in determining the nature of the X-ray absorption (Matt et al. 1997b; Matt et al. 1999). However, the PDS sensitivity (a fraction of mCrab in a typical 50 ks observation) prevented robust detections in most Seyfert 2 galaxies. Based on the BeppoSAX results, Maiolino et al. (1998) had classified the NGC 5643 nucleus as a “warm-scattered” Compton-thick AGN, obscured by $N_H \geq 10^{25} \text{ cm}^{-2}$. This classification was mainly driven by the steep, unabsorbed spectrum observed by BeppoSAX, which is inconsistent with Compton-reflection dominance. It is interesting to observe that this classification was not supported by the measurement of the K_{α} fluorescent iron line centroid, which was (and has been across the whole X-ray history of NGC 5643) inconsistent with He- or H-like iron fluorescent K_{α} transitions. XMM-Newton measured a Compton-thin absorber instead, with a column density in the range $N_H 6\text{--}10 \times 10^{23} \text{ cm}^{-2}$. The absorber either directly covers the nuclear emission, or its Compton-reflection. In the latter scenario, we might be observing reprocessing from

the inner far side of the “torus”, partly absorbed by the outer rim of its near side. This scenario would require a rather fine-tuned orientation. This, together with the lack of appropriate statistics, might explain why this kind of reflection-dominated AGN. Incidentally, the lower column density helps to substantially reduce (but not to completely reconcile) the need for a dust composition geared toward large dust grains implied by X-ray obscuration with respect to the observed narrow Br_{α} line component fluxes (Lutz et al. 2002).

The lack of detection of transmitted nuclear emission in the Compton-reflection dominated scenario might be due to the line-of-sight toward the nucleus intercepting Compton-thick matter. This may indicate that the “torus” is thicker, the closer to its mid-plane one looks (Matt et al. 2000). Alternatively, the line of sight to the nucleus during the XMM-Newton observation could be probing a transient phase of low activity. The recent serendipitous discovery of transitions between transmission- to reflected-dominated spectra of Seyfert 2 galaxies (see Matt et al. 2003, and references therein) shows that the classification of an obscured AGN as Compton-thick/-thin can be time-dependent. In at least two well studied cases (NGC 2992; Gilli et al. 2000; NGC 6300, Guainazzi 2002), these transitions are due to changes of the overall AGN output by more than one order of magnitude, on timescales of the order of a few years. The reflection-dominated state in these cases is the “echo” of a previous state of AGN activity, as in the “swan song” state of the Narrow Line Seyfert 1 galaxy NGC 4051 (Guainazzi et al. 1998; Uttley et al. 1999). Interestingly enough, earlier ASCA and BeppoSAX spectra of the NGC 5643 nucleus are markedly different in both flux and spectral shape from those observed by XMM-Newton. Taking into account the possible contamination of “source X-1” into the large ASCA and BeppoSAX aperture, the observed spectral variability is consistent with an historical dynamical range in the AGN power of one order of magnitude. Indeed, our interpretation of the steep spectrum observed by BeppoSAX is that the nucleus was outshone by NGC 5643 X-1, due to a phase of very low AGN brightness. This interesting possibility can be tested with future monitoring campaigns of this active nucleus, that we plan to pursue in the nearby future. Of course, we cannot rule out that the steep BeppoSAX spectrum is due to a revival of the AGN itself. This would make the X-ray history of NGC 5643 even more intriguing, though.

The nature of the soft X-ray (*i.e.* $\leq 2 \text{ keV}$) emission in the NGC 5643 nucleus is still uncertain. All possible models for the soft X-ray spectrum requires a contribution from emission lines. The quality of the data is, however, not good enough to establish the physical process responsible for them. A good fit is obtained with the composition of two thermal emission components from optically thin, collisionally ionized plasma, with temperatures $kT \simeq 0.15 \text{ keV}$, and $kT \simeq 0.67 \text{ keV}$. A possible origin for this emission is gas heated by shocks or winds in regions of intense star formation. The 0.5–4.5 keV luminosity associated with these thermal components ($L_{0.5\text{--}4.5 \text{ keV}} \simeq 1.4 \times 10^{40} \text{ erg s}^{-1}$) is consistent with the empirical relation discovered by David et al. (1992) with the Far InfraRed (FIR) luminosity in starburst galaxies: $\text{NGC 5643 } L_{\text{FIR}} = 1\text{--}2 \times 10^{10} L_{\odot} \simeq L_{0.5\text{--}4.5 \text{ keV}}^{0.92}$ (Genzel et al. 1998; Moran et al. 2000). On the other hand,

the 2–10 keV luminosity of the “ultra-hot” thermal component in Model#2 of Table 3 ($\simeq 5 \times 10^{39}$ erg s $^{-1}$) is only marginally consistent with the empirical relation between 2–10 keV and FIR luminosity established by Ranalli et al. (2003). Conversely, one can estimate the bolometric luminosity of the AGN in NGC 5643, $L_{bol}^{AGN} \sim 30L_X \simeq 7.5 \times 10^{42}$ erg s $^{-1}$, if it has a typical Spectral Energy Distribution as in, *e.g.*, Elvis et al. (1994) and one assumes Model#3 in Table 3. A substantial contribution of AGN reprocessing to the measured FIR luminosity would not be required. However, evidence for an intense nuclear starburst in this galaxy is still controversial. Alternatively, the EPIC soft X-ray spectrum can be fit with a pure photoionized plasma, whose signature in the optical band would be represented by the bright one-sided ionization cone (Simpson et al. 1997). In this scenario, it is ruled out that a substantial contribution to the soft X-ray emission comes from scattering of the nuclear continuum, as this would imply too steep a slope to be consistent with that inferred from the hard X-ray spectrum of this very same observation. However, it is possible to fit the soft X-ray spectrum with a pure emission-line model. High-resolution spectroscopy observations of bright Seyfert 2 galaxies have indeed shown that the contribution of scattered continuum to the photoionized emission could be negligible (Kinkhabwala et al. 2002). In this scenario the line identification is not fully unambiguous, and contamination between transitions of different elements likely. At 0th-order, the interpretations fall into two broad classes. In the first the spectrum is dominated by He-like K_α transitions of Carbon, Oxygen, and Neon, with features from the last element being particularly abundant and including as well a K_β line, and a Radiative Recombination Continuum (RRC). Interestingly enough, the centroid of the feature encompassing the OVII triplet - which EPIC data cannot resolve - is consistent with intercombination and resonant lines being the dominant contributors of the triplet, by contrast to NGC 1068. This suggests a large density ($n \geq 10^{12}$ cm $^{-3}$) for the photoionized medium (Porquet & Dubau 2000). In a second possible class of interpretations, the line spectrum is dominated by transitions of highly ionized iron species from FeXVII to FeXXIV. This interpretation would be consistent with the detection of a weak FeXXVI K_α line in the hard part of the EPIC spectrum (cf. Fig. 4). It is interesting to observe that our line deconvolution of the EPIC spectra contains all the brightest lines discovered in the high-resolution spectrum of NGC 1068 (Kinkhabwala et al. 2002), except its OVIII and NVII. OVII β is missing as well, although in this case it might be blended to invisibility with the NVII RRC.

The quest for the physical origin of the soft X-ray emission in this object requires instrumentation of enough power to be able to perform high-resolution spectroscopy in the soft X-ray regime. *Chandra* high-resolution imaging could be important as well in determining whether the soft X-ray nuclear spectrum is dominated by diffuse emission, associated to the 15'' ionization cone. AGN photoionized plasma structures extending on scales of hundreds parsecs have been observed in nearby Seyfert 2s (Sako et al. 2000; Bianchi et al. 2003; Iwasawa et al. 2003). Evidence from the XMM-Newton image is still inconclusive in this respect.

4.2 NGC 5643 X-1: an ultrabright ULX?

The XMM-Newton image of the NGC 5643 field clearly shows a source, about 0.8' NE from the position of the optical nucleus. This source - labeled “NGC 5643 X-1” in this paper - is about a factor 50 per cent brighter than the nucleus itself, and had been previously observed by the ROSAT HRI, in a three times fainter state. In Fig. 8 we show an overlap between the EPIC intensity contours and the simultaneous OM image. Although the relatively broad Point Spread Function of the XMM-Newton optics prevents us from pinpointing an unambiguous optical counterpart for NGC 5643 X-1, it is apparently located at the outskirts of the host galaxy optical extension. If the source is not a background object, its remarkable X-ray luminosity ($\simeq 4.4 \times 10^{40}$ erg s $^{-1}$) would convert it in the third brightest ULX ever observed in hard X-rays (Foschini et al. 2002; Humphrey et al. 2003; Swartz et al. 2003). Its spectral properties provide relatively little information on its nature. A fit with a simple power-law ($\Gamma \simeq 1.7$) or bremsstrahlung ($kT \simeq 8$ keV) continuum with moderate absorption ($N_H \simeq 1\text{--}2 \times 10^{21}$ cm $^{-2}$) is a good description of the observed spectrum. It is interesting to observe that a fit with a multitemperature disk blackbody is poor.

In the quest for the nature of NGC 5643 X-1 the discovery of a possible counterpart at other wavelengths would be crucial. No known radio source can be associated with the position of NGC 5643 X-1. A 2MASS bright optical source with coordinates: $\alpha_{2000} = 14^h 32^m 43.0^s$; $\delta_{2000} = -44^\circ 09' 40''$, about a factor of 3 fainter than the optical nucleus, is only marginally consistent with typical uncertainties in XMM-Newton attitude reconstruction. The brightest OM UV source in the EPIC error box has coordinates $\alpha_{2000} = 14^h 32^m 42.9^s$; $\delta_{2000} = -44^\circ 09' 34''$. The identification of an unambiguous counterpart needs to await a more precise determination of the X-ray centroid, which could be achieved with a *Chandra* observation of the galaxy field. On the other hand, the study of the X-ray history of the NGC 5643 field suggest that NGC 5643 X-1 underwent flux variations with a dynamical range of at least 5, thus ruling out an association with a supernova remnant. Again, future monitoring campaigns of this field may offer important clues on its variability pattern, and henceforth on its nature.

ACKNOWLEDGMENTS

This work is based on observations obtained with XMM-Newton, and ESA science mission with instruments and contributions directly funded by ESA Member States and the USA (NASA). This research has made use of the NASA’s Astrophysics Data System Abstract Service, and of the NASA/IPAC Extragalactic Database (NED), which is operated by the Jet Propulsion Laboratory, California Institute of Technology, under contract with the National Aeronautic and Space Administration. Last, but not least, we acknowledge careful reading and useful suggestions from an anonymous referee.

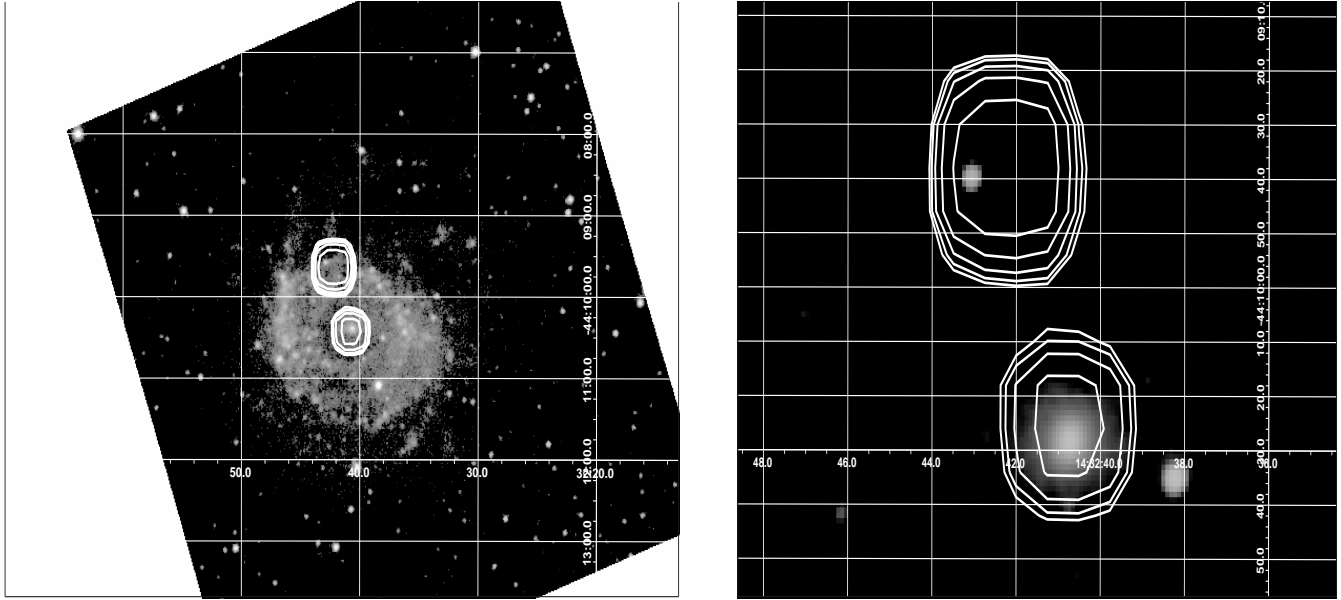


Figure 8. *Left panel* EPIC pn iso-intensity contours superposed to the innermost science window of the OM/UVW1 exposure. The contours represent 9 logarithmically scaled steps in the pixel count range between 5 and 169. *Right panel:* zoom of the innermost $1'50''$. The pn iso-intensity contours are superposed to the K-band 2MASS image

REFERENCES

- Anders E. & Grevesse N., 1989, *Geochimica et Cosmochimica Acta* 53, 197
- Antonucci R.R.J., Olszewski E.W., 1985, *AJ*, 90, 2003
- Awaki H., Koyama K., Inoue H., Halpern J.O., 1991, *PASJ* 43, 195
- Bennett C.L., et al., 2003, *ApJS*, 148, 1
- Bianchi S., Balestra I., Matt G., Guainazzi M., Perola G.C., 2003, *A&A*, 402, 141
- Brinkman A.C., Kaastra J.C., van der Meer R.J.L., Kinkhabwala A., Behar E., Kahn S., Paerels F.B.S., Sako M., 2002, *A&A*, 396, 761
- Cappi M., et al., 1999, *A&A*, 344, 857
- Cash W., 1976, *A&A*, 52, 307
- Cid Fernandes R., Heckman T., Schmitt H., González-Delgado R.M., Storchi-Bergmann T., 2001, 558, 81
- David L.P., Jones C., Forman W., 1992, *ApJ*, 388, 82
- der Herder J., Brinkman A.C., Kahn S.M., et al., 2001, *A&A*, 365, L7
- Elvis M., Lawrence A., 1988, *ApJ*, 331, 161
- Elvis M., Wilkes B.J., McDowell J.C., Green R.F., Bechtold J., Willner S.P., Oey M.S., Polowski E., Cutri R., 1994, *ApJS* 95, 1
- Fabian A.C., 1999, *MNRAS*, 308, L39
- Genzel R., Lutz D., Sturm E., et al., 1998, *ApJ*, 498, 579
- Gilli R., Maiolino R., Marconi A., et al., 2000, *A&A* 355, 485
- Guainazzi M., 2002, *MNRAS*, 329, L13
- Guainazzi M., et al., 1998, *MNRAS* 301, L1
- Guainazzi M., Matt G., Antonelli L.A., et al., 1999, *MNRAS*, 310, 10
- Guainazzi M., Matt G., Brandt W.N., et al., 2000, *A&A*, 356, 463
- Guainazzi M., Matt G., Fabian A.C., et al., *Proceedings of the Workshop "Multiwavelength AGN surveys"*, in press
- Humphrey P.J., Fabbiano G., Elvis M., Church M.J., Balucinska-Church M., 2003, *MNRAS*, 344, 134
- Koyama K., Inoue H., Tanaka Y., Awaki H., Takano S., Ohashi T., Matsuoka M., 1989, *PASJ*, 41, 731
- Jansen F., et al., 2001, *A&A* 365, L1
- Kewley L.J., Heisler C.A., Dopita M.A., Sutherland R., Norris R.P., Reynolds J., Lumsen S., 2000, *ApJ*, 530, 704
- Kinkhabwala A. et al., 2002, *ApJ*, 575, 732
- Iwasawa K., Wilson A.S., Fabian A.C., Young A.J., 2003, *MNRAS*, 345, 369
- Lampton M., Margon B., Bowyer S., 1976, *ApJ*, 207, 894
- Lumb D.H., Warwick R.S., Page M., De Luca A., 2002, *A&A*, 389, 93L
- Lutz D., Maiolino R., Moorwood A.F.M., Netzer H., Wagner S.J., Sturm E., Genzel R., 2002, *A&A*, 396, 439
- Magdziarz P. & Zdziarski A.A., 1995, *MNRAS* 273, 837
- Maiolino R., Salvati M., Bassani L., Dadina M., della Ceca R., Matt G., Risaliti G., Zamorani G., 1998, *A&A* 338, 781
- Mason L., et al., 2001, *A&A*, 365, L36
- Matt G., et al., 1997a, *A&A*, 325, L13
- Matt G., et al., 1999, *A&A* 341, L39
- Matt G., Fabian A.C., Guainazzi M., Iwasawa K., Bassani L., Malaguti G., 2000, *MNRAS* 318, 173
- Matt G., Fabian A.C., Reynolds C., 1997b, *MNRAS*, 289, 175
- Matt G., Guainazzi M., Maiolino R., 2003, *MNRAS*, 342, 422
- Mewe R., Gronenschild E.H.B.M., van der Oord G.H.J., 1985, *A&AS*, 62, 197
- Moran E.C., Barth A.J., Kay L.E., Filippenko A.V., 2000, *ApJ* 540, L73
- Morris S., Ward M., Whittle M., Wilson A.S., Taylor K., 1985, *MNRAS*, 216, 193
- Nandra K., George I.M., Mushotzky R.F., Turner T.J., Yaqoob T., 1997, *ApJ* 467, 70
- Perola G.C., Matt G., Cappi M., Fiore F., Guainazzi M., Maraschi L., Petrucci P., Piro L., et al., 2002, *A&A*, 389, 202
- Porquet D., Dubau J., 2000, *A&AS*, 143, 495
- Ranalli P., Comastri A., Setti G., 2003, *A&A*, 399, 39
- Reeves J.N., Turner M.J.L., 2000, *MNRAS*, 316, 234
- Phillips M.M., Charles P.A., Baldwin J.A., 1983, *ApJ*, 266, 485
- Risaliti G., Maiolino R., Salvati M., 1999, *ApJ* 522, 157
- Sako M., Kahn S.M., Paerels F., Liedahl D.A., 2000, *ApJL* 543, L115
- Simpson C., Wilson A.S., Bower G., Heckman T.M., Krolik J.H.,

- Miley G.K., 1997, 474, 121
Strüder L., et al., 2001, A&A 365, L18
Swartz D.A., Ghosh K.K., Tennant A.F., 2003, AAS, 202, 1109
Turner T.J., George I.M., Nandra K., Mushotzky R.F., ApJ 488,
164
Turner M.J.L., et al., 2001, A&A 365, L27
Ueno S., Mushotzky R.F., Koyama K., Iwasawa K., Awaki H.,
Hayashi I., et al., 1994, PASJ, 46, L71
Uttley P., McHardy I., Papadakis I.E., Guainazzi M., Fruscione
A., 1999, MNRAS 307, L6
Vignati P., Molendi S., Matt G., et al., 1999, A&A, 349, L57
Warwick R.S., Koyama K., Inoue H., Takano S., Awaki H., Hoshi
R., 1989, PASJ, 41, 739
Wilman R.J., Fabian A.C., 1999, MNRAS, 309, 862